COBEM 2023 27TH INTERNATIONAL CONGRESS OF MECHANICAL ENGENEERING

ABCM Brazilian Society of Mechanical Sciences and Engineering
27th ABCM International Congress of Mechanical Engineering
December 04-08, 2023, Florianópolis-SC, Brazil

COB-2023-0571
CHAOS CONTROL OF A NONLINEAR PENDULUM USING AN ACTIVE DISTURBANCE REJECTION APPROACH

Alessandro Rosa Lopes Zachi[1a]
Josiel Alves Gouvêa[1b]
Aline Souza de Paula[3]
Marcelo Amorim Savi[4]

[1]Centro Federal de Educação Tecnológica Celso Suckow da Fonseca - CEFET/RJ
[a]Programa de Pós-graduação em Engenharia Elétrica (PPEEL), Av. Maracanã 229, 20.271-110 - Maracanã, Rio de Janeiro, RJ, Brazil.
[b]Núcleo de Pesquisa em Mecatrônica (NUPEM), Estrada de Adrianópolis 1317, 26.041-271 - Santa Rita, Nova Iguaçu, RJ, Brazil.
e-mails: alessandro.zachi@cefet-rj.br, josiel.gouvea@cefet-rj.br

[3]University of Brasília – UnB, Department of Mechanical Engineering, 70.910-900 - Brasília, DF, Brazil.
e-mail: alinedepaula@unb.br

[4]Federal University of Rio de Janeiro, COPPE - Mechanical Engineering
Center for Nonlinear Mechanics, 21.941.972 - Rio de Janeiro, RJ, Brazil.
e-mail: savi@mecanica.coppe.ufrj.br

Abstract: *Chaos control has the objective of stabilizing unstable periodic orbits (UPOs) embedded in a chaotic attractor. Since these orbits belong to the system dynamics, this approach has several advantages compared to other controller processes. This paper investigates the utilization of a modified Active Disturbance Rejection Control (ADRC) method to stabilize UPOs. This method is well-known in the literature for its ability to reject external disturbances, compensating for parametric uncertainties. It is composed of an extended observer that estimates the system state variables and unobserved signals used in a state feedback control law. The main feature of the modified ADRC scheme compared to the standard ones is that the former does not require exact knowledge of the control coefficient, which increases its robustness to a wide class of parametric uncertainties.*

Keywords: *Chaos control, Unstable periodic orbits, Robust control, MP-ADRC method.*

1. INTRODUCTION

Chaos control exploits the essential characteristic of dynamical systems to perform the stabilization of target orbits. Since chaos is characterized by the existence of an infinite number of unstable periodic orbits (UPOs) embedded in chaotic attractor, chaos control uses these orbits as targets, which makes this approach low energy consumption since it is related to tiny perturbations. Under this condition, a dynamical system adopting chaotic regimes becomes interesting due to the wide range of potential behaviors being related to a flexible design. This idea makes chaos desirable in different applications that varies in distinct areas including mechanics, electronics (Luo *et al.*, 2022), aerospace, robotics and biomechanics.

Several approaches were employed to perform UPO stabilization. Since the pioneer work of the OGY method (Ott *et al.*, 1990), several discrete methods were developed, promoting actuation in some Poincare section. In this regard, it is important to highlight the semi-continuous method (Hübinger *et al.*, 1994), and the multiparameter method (de Paula and Savi, 2009). Concerning the continuous methods, it is important to mention the extended time-delayed feedback control (ETDF) (Socolar *et al.*, 1994) that is a generalization of the classical time-delayed feedback control (TDF) (Pyragas, 1992). de Paula and Savi (2011) discussed a comparative analysis of the main chaos control methods.

Kapitaniak (1992) applied nonfeedback methods by adding a controller, which consists in a linear oscillator, to the dynamical system with the help of coupling elements. Recently, adaptive synchronization control of chaotic systems based on Takagi-Sugeno (TS) fuzzy models has received several contributions in the scientific literature. For instance, Bessa *et al.* (2009, 2012) proposed an adaptive fuzzy sliding mode strategy enhanced by an adaptive fuzzy algorithm to cope with modeling inaccuracies. The method is applied in other to stabilize UPOs embedded in chaotic response as well as generic orbits. (Zeng *et al.*, 2019) proposed an adaptive scheme for synchronization of TS fuzzy chaotic system with unknown parameters. Zhu *et al.* (2020) investigated an adaptive synchronization method for chaotic systems also based on TS fuzzy model but applied to systems with time-delay. Luo *et al.* (2022) investigated the chaos control problem

of microelectromechanical system (MEMS) resonators by using the analog circuits. For suppressing harmful chaotic oscillation, an adaptive control scheme was proposed and the results were verified by an analog circuit consisting of an error module, a parameter update module and a control input module. This paper presents a Modified-Plant Active Disturbance Rejection Control (MP-ADRC) method (Zachi *et al.*, 2019; Gouvêa *et al.*, 2023) to perform chaos control. This approach is a modified version of the standard ADRC method introduced by Jingqing (1998) and then improved by Madoński *et al.* (2015). A nonlinear pendulum is discussed as a case study (de Paula and Savi, 2011). Results show that the controller is able to stabilize UPOs, being robust against uncertainties in the system's parameters.

The paper is organized as follows. In Section 2. the control problem is stated as the output tracking control of a target reference trajectory. The methodology for solving the stabilization problem of unstable chaotic orbits is also discussed in this section. The nonlinear pendulum model is presented in Section 3. followed by the statement of the system error dynamics in Section 4. The design of the MP-ADRC scheme for the system is presented in Section 5. and the stability is discussed in Section 6. The simulation tests and the obtained results are explained in Section 7. followed by the work concluding remarks in Section 8.

2. PROBLEM STATEMENT

This work considers the control problem addressed to a nonlinear pendulum mechanism of Fig. 1. It consists in a relevant challenging application for the chaos control method due to its known high instability motion characteristics. The problem is analyzed from a theoretical point of view, since the dynamics of the pendulum can be described by a general class of second-order nonlinear systems given by

$$\ddot{y}(t) + a_1 \dot{y}(t) + a_0 y(t) = b_p u(t) + h(\dot{y}(t),\ y(t))\,, \tag{1}$$

in which $y(t) \in \mathbb{R}$ represents the system output variable, $u(t) \in \mathbb{R}$ represents the system input variable (control signal) and $h(\dot{y},\ y) \in \mathbb{R}$ denotes the nonlinear functions and/or non measurable states. The constants $a_0,\ a_1,\ b_p \in \mathbb{R}$ are the system's parameters. The control objective is to design a control law for $u(t)$ in order to force the output $y(t)$ to converge asymptotically to a desired reference trajectory given by $y^*(t)$. For the pendulum mechanism, $y(t)$ represents the angular position of the disk, in rad, and $u(t)$ represents a vertical linear displacement, in meters, generated by a vertical linear actuator which pulls up and down one of the side strings of the mechanism to stabilize the pendulum according to a desired stable orbit $(y^*(t), \dot{y}^*(t))$. If the system's output error is defined as

$$e(t) := y(t) - y^*(t)\,, \tag{2}$$

then the current tracking control problem can also be stated as

$$\lim_{t\to\infty} e(t) \to 0\,. \tag{3}$$

This work proposes a solution based on the MP-ADRC method reported in Zachi *et al.* (2019). It is a variant approach of the standard-ADRC originally proposed by Jingqing (1998) and further improved in Madoński *et al.* (2015). It is worth mentioning that the use of ADRC-based control methods are appliable when there are parametric uncertainties in the system's parameters a_1, a_0, b_p, and others, and/or when there are non measurable variables that need to be determined for compensation purposes. For dealing with the cited drawback, ADRC-based schemes, such as the ones reported by Madoński *et al.* (2015); Lu *et al.* (2021); Wu *et al.* (2022), propose the use of an Extended State Observer (ESO) for estimating the system's state variables and also the function f, and use them to compose a feasible version. To simplify the presentation and the mathematical developments, henceforth the time dependency notation will be dropped. In this way, throughout the text, the equivalent notations like $y \equiv y(t)$, are adopted. The terms "system" and "plant" are also adopted to denote the dynamical system or the set of differential equations that describe it.

In the next sections, the analysis and design procedures of the MP-ADRC method applied to the nonlinear pendulum mechanism are discussed.

3. THE PENDULUM MATHEMATICAL MODEL

This paper investigates a mechanical nonlinear pendulum that consists of an aluminum disc with a lumped mass driven by a string-spring device that is attached to an electric motor that provides either external stimulus or torsional stiffness. An illustrative image of the system is shown in Fig.1. Also, there is a magnetic device that provides adjustable energy dissipation. A mathematical model is developed presenting numerical simulations of the uncontrolled system which demonstrates a close agreement with experimental data (de Paula *et al.*, 2006). The mathematical model for the pendulum dynamics describes the time evolution of the angular position ϕ [rad], assuming that w, [rad/s] is the forcing frequency, I [kg m^2] is the total inertia of rotating parts, k [N/m] is the spring stiffness, ζ [kg m^2 s^{-1}] represents the viscous damping coefficient, μ [N m] is the dry friction coefficient, m [kg] is the lumped mass, a [m] defines the position of the string guide

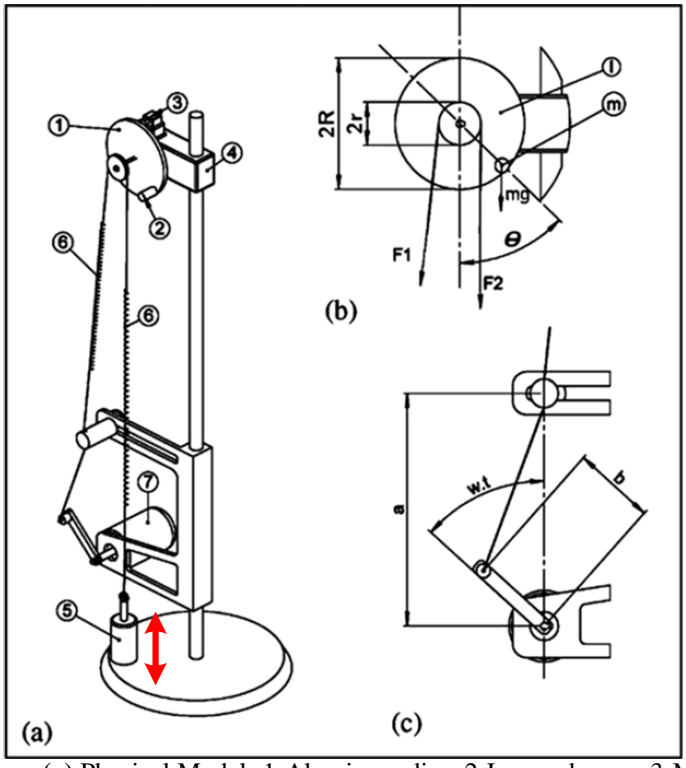

Figure 1: Nonlinear pendulum. **(a)** Physical Model. 1-Aluminum disc; 2-Lumped mass; 3-Magnetic damping device; 4-Rotary Motion Sensor; 5-Actuator; 6-String-spring device; 7-Electric motor. **(b)** Parameters and forces on the aluminum disc. **(c)** Parameters from driving device (Pereira-Pinto *et al.*, 2004).

with respect to the motor, b [m] is the length of the excitation arm of the motor, D [m] is the diameter of the metallic disc, and d [m] is the diameter of the driving pulley. According to de Paula *et al.* (2006), the equation of motion is governed by:

$$\ddot{\phi} + \frac{\zeta}{I}\dot{\phi} + \frac{kd^2}{2I}\phi = \frac{kd}{2I}\left[\Delta_f(t) - \Delta_{l1}\right] - \frac{mgD\sin(\phi)}{2I} - \frac{2\mu\arctan(q\dot{\phi})}{\pi I}, \tag{4}$$

$$\Delta_f(t) = \sqrt{a^2 + b^2 - 2ab\cos(\omega t)} - (a - b), \tag{5}$$

in which Δ_{l1} [m] is the displacements that represents the control input (de Paula *et al.*, 2006); q is a sufficiently large positive constant for modeling the dry friction in the continuous form (Leine, 2000). It is noticeable that the equation of motion is an ODE with a linear part on the left-hand side of Eq. (4) and state-dependent and input-dependent nonlinear terms on its right-hand side.

4. ERROR DYNAMICS

The main idea of the Modified ADRC proposal (Zachi *et al.*, 2019) is to introduce a structural transformation in the input/output system description in order to obtain a new dynamical equation with a desired structural feature. This particular structure sought not only facilitates the controller design procedures, but also helps to relax the condition of exact or approximate knowledge on the values of some plant parameters. As will be shown later, such dynamical transformation does not affect the control objectives outlined for the original plant.

Based on the expression of Eq. (2), the error variable e can be define as

$$e = \phi - \phi^* . \tag{6}$$

It is not difficult to verify that its second-order time derivative, according to Eq. (4), is given by

$$\ddot{e} = -\frac{\zeta}{I}\dot{\phi} - \frac{kd^2}{2I}\phi + \frac{kd}{2I}\Delta_f - \frac{mgD\sin(\phi)}{2I} - \frac{2\mu\arctan(q\dot{\phi})}{\pi I} - \frac{kd}{2I}\Delta_{l1} - \ddot{\phi}^* . \tag{7}$$

4.1 MP-ADRC formalism

Only for the controller design convenience, let us rewrite the dynamics of Eq. (7) as follows:

$$\begin{cases} \ddot{e} \;=\; -\dfrac{kd}{2I}\Delta_{l1} \;+\; f(\phi,\; \dot{\phi},\; \ddot{\phi}^*)\,, \\ f(\phi,\; \dot{\phi},\; \ddot{\phi}^*) = \; -\dfrac{\zeta}{I}\,\dot{\phi} - \dfrac{kd^2}{2I}\,\phi + \dfrac{kd}{2I}\Delta_f - \dfrac{mgD\sin(\phi)}{2I} - \dfrac{2\mu\arctan(q\dot{\phi})}{\pi I} \;-\; \ddot{\phi}^*\,. \end{cases} \tag{8}$$

In Eq. (8), note that $f(\phi,\; \dot{\phi},\; \ddot{\phi}^*)$ gathers all the system's state variables and their coefficients, the nonlinear functions, and other variables of the original error dynamics. The format presented in Eq. (8) follows the formalism of the ADRC method and, in such approach, $f(\phi,\; \dot{\phi},\; \ddot{\phi}^*)$ figures out as a *disturbance term*. In the following developments, only for the sake of simplicity, $f(\phi,\; \dot{\phi},\; \ddot{\phi}^*)$ is denoted by f_ϕ, the term $-(kd/2I)$ by K_p, and the term Δ_{l1} by u_1. Then, Eq. (8) henceforth assumes the following form:

$$\ddot{e} \;=\; K_p u_1 \;+\; f_\phi\,. \tag{9}$$

In this way, the nonlinear ODE of the original system, describe by Eqs. (4) and (5), is now represented by a second-order linear ODE of Eq. (9), with an input variable u_1 and also an input disturbance term f_ϕ.

4.2 Control rationale

By thinking of a scenario in which the system of Eq. (9) is linear but subjected to a nonlinear disturbance term f_ϕ, then the control problem of stabilizing it could be solved by choosing u_1 as

$$u_1 = \left(\frac{1}{K_p}\right)\left[-f_\phi + v^*\right], \tag{10}$$

in which $v^* \in \mathbb{R}$ denotes some efficient control strategy. If u_1 is feasible, then the closed-loop error system becomes

$$\ddot{e} \;=\; v^*\,, \tag{11}$$

which is a linear ODE from v^* to e. Nevertheless, if the function f_ϕ is not available, then the designer will face some difficulties to realize Eq. (10) directly. In addition, another condition that needs to be assured is the exact value of the control coefficient K_p, whose inverse is also needed. This control design difficulties can be overcome by employing the Modified-Plant Active Disturbance Rejection Control (MP-ADRC) Method (Zachi *et al.*, 2019).

5. MP-ADRC APPLIED TO THE PENDULUM SYSTEM

In this section, the design procedures of the MP-ADRC method are presented and discussed. Before going into the developments, some fundamental hypothesis about the plant in Eqs. (4) and (5) need to be assumed.

5.1 Fundamental Assumptions

(A1) The plant variables ϕ and $\dot{\phi}$ are measurable;

(A2) The reference variables ϕ^* and $\dot{\phi}^*$, that represent the desired orbit, are smooth, measurable, and bounded.

(A3) The plant parameter $kd/2I$ is constant and has known sign.

Assumptions (A1) and (A2) are assumed for simplicity. Assumption (A3) is needed for the controller design via the MP-ADRC method. This assumption is less restrictive than assuming the exact knowledge of the cited plant parameter.

5.2 Preliminaries

In the following developments, frequency domain and time domain notations are used in mixed form. Such kind of presentation is adopted here only for analysis purposes. In the field of linear time-invariant systems, time domain is related to frequency domain by the Laplace Transform operator $\mathcal{L}$. Thus, for example, assuming null initial conditions, time derivatives and integrals of a certain function $x(t)$ are denoted, respectively, by

$$x(t) \;\xrightarrow{\mathcal{L}}\; X(s)\,, \qquad \mathcal{L}\{\dot{x}(t)\} = s\,X(s)\,, \qquad \mathcal{L}\left\{\int x(t)\,dt\right\} = \frac{1}{s}\,X(s)\,,$$

in which $X(s)$ is the Laplace Transform of variable $x(t)$. The term 's' is the Laplace variable and its power represents the degree of differentiation of $x(t)$ in time. The same holds for integrals that are represented by '$1/s$'. Our interest is to quickly identify important relationships and/or solve algebraic manipulations by using polynomials (frequency domain) instead of ODEs (time domain). However, an important issue worth mentioning is that some time domain quantities may not possess a frequency domain representation, such as the general nonlinear functions of the plant states inside f_ϕ, for example. Despite, this last issue, we believe that the mixed notation form represents the most suitable mathematical formalism for the analysis and design in this work.

5.3 Developments

The basic implementation of the MP-ADRC method is depicted in Fig. 2. In the illustrative diagram, one can note that the method uses only the system's error variable e for producing an auxiliary variable z. In this context, z has no physical meaning and only serves as a mathematical artifact to develop the strategy toward reaching important expressions for the controller design. By using the auxiliary variable z to feed the ESO, the latter one then 'observes' a *modified plant*. The advantages of such modification are discussed in the following.

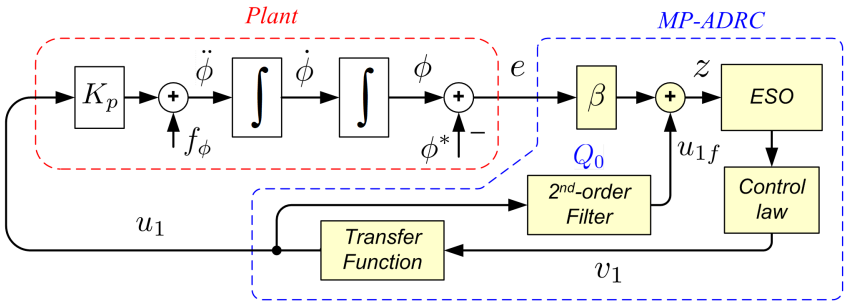

Figure 2: MP-ADRC implementation diagram.

The plant modification is introduced by two main blocks: the constant gain $\beta \in \mathbb{R}$; and a linear second-order filter transfer function, both given by

$$\beta := K_0 \; sign(K_p)\,, \quad K_0 > 0\,, \qquad Q_0(s) = \frac{s}{(s+\alpha)^2}\,, \quad \alpha > 0\,, \qquad \longrightarrow \qquad u_{1f} = Q_0(s)\; u_1\,, \tag{12}$$

in which K_0 and α are real design constants. Thus, the time and frequency domain representations of the auxiliary variable z are given, respectively by

$$z \;= \beta e \;+\; u_{1f}\,, \qquad \xrightarrow{\mathcal{L}} \qquad z = \beta\; e \;+\; \frac{s}{(s+\alpha)^2}\; u_1\,, \tag{13}$$

After manipulating the frequency domain expression in Eq. (13), we obtain

$$(s+\alpha)\; z = \underbrace{\beta(s+\alpha)}_{\Omega(s)}\; \eta \;+\; \underbrace{\frac{s}{(s+\alpha)}\; u_1}_{v_1}\,, \tag{14}$$

which is equivalent to the following time-domain ODE:

$$\dot{z} + \alpha z = \Omega + v_1\,, \tag{15}$$

Note that Eqs. (9) and (15) are similar. The main feature of Eq. (15) compared to Eq. (9) is the presence of the control variable v_1 with a unitary coefficient. This represents an advantage for the control law design of v_1 since henceforth it does not require the knowledge of K_p^{-1}. Indeed, in this case, once the internal dynamics (or the homogeneous part) of the ODE in Eq. (15) is stable by construction, a viable control law for stabilizing it would be chosen as $v_1 = -\Omega$. However, due to the unavailability of Ω, an Extended State Observer (ESO) is always required for estimating $\hat{\Omega}$, and then use it in the following realizable control law:

$$v_1 \;=\; -\hat{\Omega}\,. \tag{16}$$

5.4 The design of the Extended State Observer (ESO)

The design of the ESO starts from the error dynamics in Eq. (15). The system's state vector is defined as $X = [z,\; \Omega]^T$, in which the disturbance term Ω is considered as an extended state variable. In this case, a third-order ESO, described by the states $\hat{X} = [\hat{X}_1,\; \hat{X}_2,]^T$, is required. Based on the previous state vector definitions, the state-space descriptions of both plant and ESO are given by:

$$\text{Plant:} \begin{cases} \dot{X} &= \begin{bmatrix} -\alpha & 1 \\ 0 & 0 \end{bmatrix} X + \begin{bmatrix} 1 \\ 0 \end{bmatrix} v_1 + \underbrace{\begin{bmatrix} 0 \\ 1 \end{bmatrix}}_{\Gamma} \dot{\Omega}\,, \\ y_z &= \begin{bmatrix} 1 & 0 \end{bmatrix} X \end{cases} \tag{17}$$

$$\text{ESO:} \begin{cases} \dot{\hat{X}} &= \underbrace{\begin{bmatrix} -\alpha & 1 \\ 0 & 0 \end{bmatrix}}_{A} \hat{X} + \underbrace{\begin{bmatrix} 1 \\ 0 \end{bmatrix}}_{B} v_1 + \underbrace{\begin{bmatrix} L_1 \\ L_2 \end{bmatrix}}_{L} e_y \,, \qquad e_y = y_z - \hat{y}_z \,, \\ \hat{y}_z &= \underbrace{\begin{bmatrix} 1 & 0 \end{bmatrix}}_{C} \hat{X} \,, \end{cases} \tag{18}$$

In Eq (18), e_y is the ESO's output error, and $L \in \mathbb{R}^3$ is the gain vector that stabilizes the ESO. By defining the vector of state estimation errors as $e_x = X - \hat{X}$, then we can compute the ESO's error dynamics from Eqs. (17) and (18), that is,

$$\dot{e}_x = \dot{X} - \dot{\hat{X}} = Ae_x + \Gamma\dot{\Omega}(t) - LCe_x \,, \quad \longrightarrow \quad \begin{cases} \dot{e}_x = \underbrace{(A - LC)}_{A_m} e_x + \Gamma\dot{\Omega}(t) \,, \\ e_y = Ce_x \,. \end{cases} \tag{19}$$

In Eq. (19), $A_m = (A - LC) \in \mathbb{R}^{2\times 2}$ stands for the ESO's closed-loop error matrix. By assigning $\dot{\Omega} \equiv 0$, the Eq. (19) can be stabilized by conveniently placing the characteristic roots of A_m in the open left complex semi-plane. This can be achieved by choosing the entries of vector L to satisfy the following expression:

$$\det\left[sI - A_m\right] = (s + w_0)^2 \,, \quad w_0 > 0 \,, \tag{20}$$

in which $w_0 \in \mathbb{R}$ is the absolute value for the ESO's characteristic roots. Both sides of Eq. (20) can be expanded in order to obtain:

$$s^2 + (L_1 + \alpha_3)s + L_2 \;=\; s^2 + 2w_0 s + w_0^2 \,, \qquad \longrightarrow \qquad L_1 = 2w_0 - \alpha_3 \,, \qquad L_2 = w_0^2 \,. \tag{21}$$

Since $\hat{X}_2$ tends to be the best estimate of Ω, it can be used to compute the control law in Eq. (16), that is

$$v_1 \;=\; -\hat{X}_2 \,. \tag{22}$$

Thus, by choosing the values of $L_1,\ L_2$ as in Eq. (21), the stability of the ESO's internal dynamics can be always guaranteed. Note, however, that once the law of v_1 has been established, it can be now used to compute the real control u_1. Let us initially consider the ESO's error $e_{x2} = \Omega - \hat{X}_2$. Since Eq. (19) is linear, the analysis of the ESO's transfer function $H(s)$ that relates variables $\dot{\Omega}$ and e_{x2}, can be accomplished by using the well-known formula (Ogata, 2010):

$$H(s) = C^*(sI - A^*)^{-1}B^* + D^* \,, \tag{23}$$

in which $A^*,\ B^*,\ C^*,\ D^*$ are the state-space matrices of a general linear system. For computing $H(s)$ in the current analysis, one needs to assign $A^* = A_m$, $B^* = \Gamma$, $C^* = [0\ 1]$ and $D^* = 0$. The matrix C^* assumes this form since the transfer function output e_{x2} is the third entry of vector e_x in Eq. (19). After performing the computation of Eq. (23), the following relation is obtained:

$$e_{x2} = H(s)\,\Omega \,, \quad \longrightarrow \quad H(s) = \frac{s^2 + (L_1 + \alpha_3)s}{s^2 + (L_1 + \alpha_3)s + L_2} \,. \tag{24}$$

Equation (24) can be simplified even more by replacing the definition of e_{x2} at the left-hand side. Thus, after manipulating such equations, a new expression arises that reveals the relation between the real disturbance term $\Omega(t)$ with its estimate $\hat{X}_3$, namely:

$$\hat{X}_2 \;=\; \underbrace{\left(\frac{w_0}{s + w_0}\right)^2}_{M(s)} \Omega \,. \tag{25}$$

Equation (25) reveals a second-order transfer function relating $\hat{X}_2$ to Ω, in frequency domain. It means that if $w_0 \to \infty$ then $M(s) \to 1$ and $\hat{X}_2 \to \Omega$. This is the theoretical perfect matching condition that corresponds to the ideal case. Nevertheless, in practice, it is only possible to assume w_0 to be sufficiently large enough for assuming $M(s) \approx 1$, which implies $\hat{X}_2 \approx \Omega$. For deriving an expression for the real control law u_1 in Eq. (9), let us focus our attention in Eqs. (14), (22) and (25) to help in the following manipulation:

$$v = -\hat{X}_2 \;= -\left(\frac{w_0}{s + w_0}\right)^2 \Omega \;= -\left(\frac{w_0}{s + w_0}\right)^2 (s + \alpha)\beta e \,. \tag{26}$$

Since the relation between v_1 and u_1 in Eq. (14) is invertible then, after performing it, we finally have that

$$u_1 = -\left[\frac{w_0^2\beta(s + \alpha)^2}{s(s + w_0)^2}\right] e \,. \tag{27}$$

As can be observed from Eq. (27), the control law u_1 is completely realizable and only depends on the design parameters w_0, α, and $\beta = K_0\ sign(K_p)$.

6. STABILITY ANALYSIS

This section discusses the stability and convergence properties of the overall control system composed of the plant in Eqs. (9) and (22), the ESO in Eqs. (18) and (21), and of the control law in Eq. (27). For this purpose, the block diagram of Fig. 2 is redrawn and reproduced in Fig. 3.

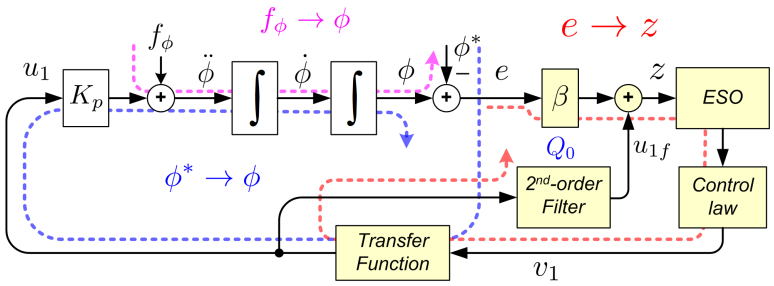

Figure 3: Stability and boundedness properties of the closed-loop system's variables.

6.1 Plant's output error convergence

The convergence property of the main interest is the study of the loop $\phi^* \to \phi$. In the ideal case, the equivalent gain of the transfer function that relates ϕ^* and ϕ should yield unity value, that is, $\phi^* = \phi$. In the most general case, this function is expected to have a gain ≈ 1. The transfer function from $f(t)$ to ϕ represents the rejection path. In the ideal case, this function should assume a value very close to zero. In the real case, this transfer function is only expected to result in an equivalent value sufficiently small and compatible with strong attenuation. After replacing the expression of Eqs. (22), (25) in Eq. (13), and gathering together similar terms with the help of Eq. (24), the following expression is obtained:

$$z \;=\; P(s)\,\beta\,e\,, \qquad P(s) = \left[1 - \frac{w_0^2}{(s+w_0)^2}\right]. \tag{28}$$

Since $P(s)$ has a bounded norm in the frequency domain, then a bounded e will result in a bounded z. As expected, this result is directly related to the convergence property of the plant's output error e. Now, consider the transfer function $\phi^* \to \phi$. In the diagram of Fig. 2, the superposition principle is applied by setting $f_\phi \equiv 0$. The searched transfer function is then calculated with the help of Eq. (27). Thus, after replacing all the control and ESO structures in the block diagram of Fig. 2, the following transfer function arise:

$$\phi \;=\; \underbrace{\left(\frac{K_0|K_p|w_0^2(s+\alpha)^2}{s^3(s+w_0)^2 + K_0|K_p|w_0^2(s+\alpha)^2}\right)}_{M(s)}\phi^*\,, \qquad f_\phi = \underbrace{\left(\frac{K_p\,s(s+w_0)^2}{s^3(s+w_0)^2 + K_0|K_p|w_0^2(s+\alpha)^2}\right)}_{N(s)}\phi\,. \tag{29}$$

There always exist sets of values for $K_0 > 0$, $w_0 > 0$, and $\alpha > 0$ that satisfy the stability condition of the transfer function $M(s)$ in Eq. (29). Zachi *et al.* (2019) established a step-by-step algorithm for choosing such design parameters. Once K_0 is fixed in a sufficiently large constant, it is not difficult to verify that the equivalent gain of $|M(s)|$ tends to 1 as w_0 increases toward ∞. This can be carried out by using frequency domain methods (Ogata, 2010). This is not the case of $|N(s)|$ which decreases in the same situation. In the literature, there is a theoretical agreement that, in general, both convergence and rejection features can be improved by increasing the value w_0. However, there are some other conditions and trade-offs that need to be analyzed previously, as argued by Gouvêa *et al.* (2023).

6.2 Parameter Tuning procedures

The convergence and rejection properties of the closed-loop system depend on the convenient choices of parameters w_0, α and K_0. The constant w_0 can be chosen arbitrarily large while respecting some limiting factors. A very important one is related to the practical implementation of the proposed controller, either by simulation or by a real hardware device: the sampling period h [seconds]. In order to avoid instability due to the divergence of numerical methods, the parameter w_0 can be chosen large enough but cannot reach or exceed the value $1/h$. For parameters α and K_0, the designer needs to choose them in order to satisfy the stability condition for the transfer function of Eq. (29) (Ogata, 2010) : the real parts of the transfer function's poles must be strictly negative. As a second step, choose α in the interval $]0; 2]$, as a first guess, and keep it fixed. Then, start choosing K_0 to satisfy the stability condition. The value of α can be updated in order to choose a more adequate value for K_0.

7. NUMERICAL SIMULATIONS

This section presents numerical simulations of the pendulum dynamics subjected to the control law of Eq. (27). The pendulum parameters are extracted from de Paula and Savi (2011), defined to ensure the chaotic behavior, being presented in Table 1. Numerical simulations are performed considering $h = 2\pi/(\omega N_m) = 0.0093\ s$ with $N_m = 120$. Figure 4 shows the uncontrolled chaotic response in phase space, accompanied by the corresponding Poincaré map.

Table 1: Simulation parameters.

Pendulum System.		
Parameter	Value	Unit
a	0.16	m
b	0.06	m
d	0.048	m
D	0.095	m
m	0.0147	kg
I	0.0001738	kg m^2
k	2.47	N/m
ζ	0.00002368	kg m^2 s^{-1}
μ	0.0001272	N m
ω	5.61	rad/s
g	9.8	m/s^2
MP-ADRC Controller.		
ω_0 $(*)$	107.52	rad/s
α	0.4374	–
K_0	0.0260	–

$(*)$ $w_0 = (1/h) - 1$.

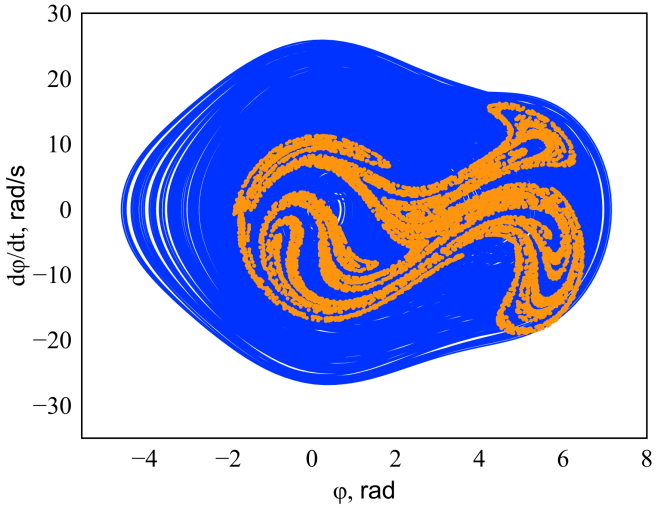

Figure 4: Chaotic response with strange attractor.

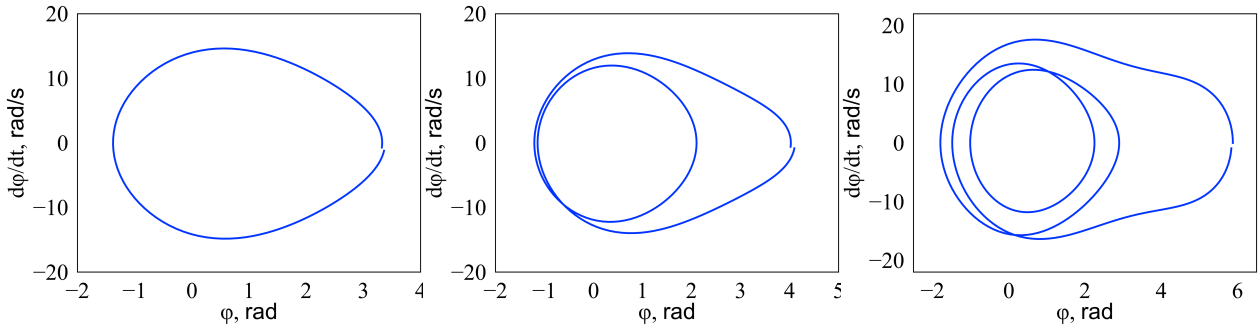

(a) Period-1. (b) Period-2. (c) Period-3.

Figure 5: Identified unstable periodic orbits.

Chaos control is a two stage approach and therefore, it is necessary to start with the learning stage where the unstable periodic orbits (UPOs) embedded in chaotic attractor are identified and controller parameters defined. UPO identification is performed by using the close return method reported by Auerbach *et al.* (1987) and de Paula and Savi (2011). In the current work, Period-1, Period-2 and Period-3 UPOs are identified, as depicted in Figure 5. These UPOs are chosen for conducting simulation tests to evaluate the effectiveness of the proposed controller.

Afterward, stabilization stage is in focus, using some target UPOs. Controller parameters are presented in Table 1. The control is applied for stabilizing the chosen UPOs: Period-1, Period-2 and Period-3. For comparison purposes, it is also considered a general orbit that does not belong to the system dynamics $(\phi_a, \dot{\phi}_a)$ defined by the ellipse equation in phase space: $\phi_a = 1.0 + 2.35\sin(2\pi t)$ [rad] and $\dot{\phi}_a = 4.70\pi\cos(2\pi t)$ [rad/s].

Figure 6 presents the controlled orbits showing the phase space, the time history and the control effort. It is shown that the controller is able to stabilized the target UPO with low power consumption. This is evident when a comparison with the general target orbit is established, showing that the control effort is much bigger. Figure 7 presents the system evolution changing from one UPO to the other. The controller process started with a chaotic behavior with the control turned off. It is then turned on to stabilize the period-1 UPO, then turned off again. It follows to stabilize the period-2 UPO and then turned off. Finally, turned on to stabilize the Period-3 orbit. It is noticeable that the MP-ADRC controller has shown to be able to achieve the objective of stabilizing the target orbits, including UPOs and a general orbit.

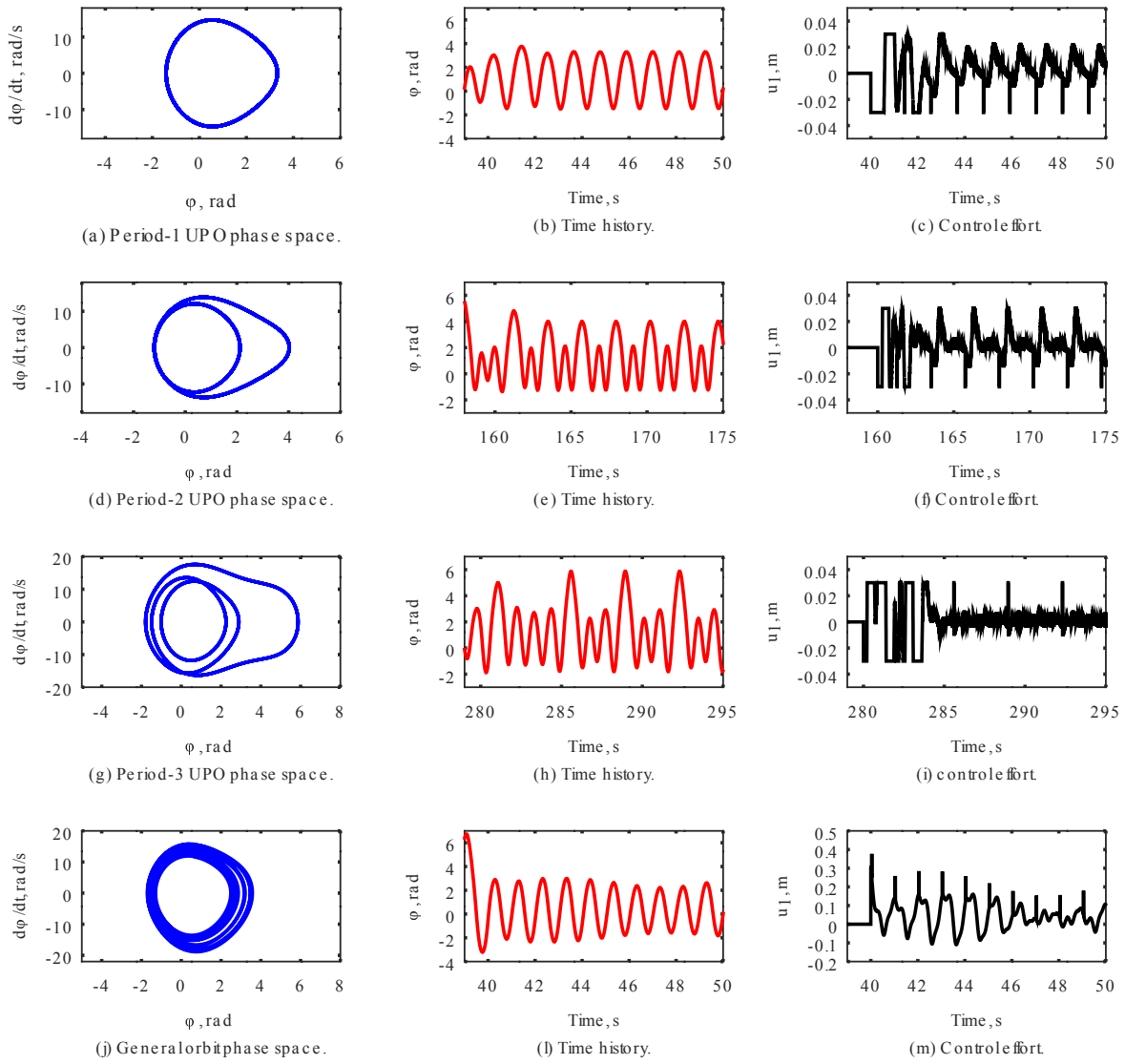

Figure 6: Stabilization of UPOs of Period-1, Period-2, Period-3, and a general orbit.

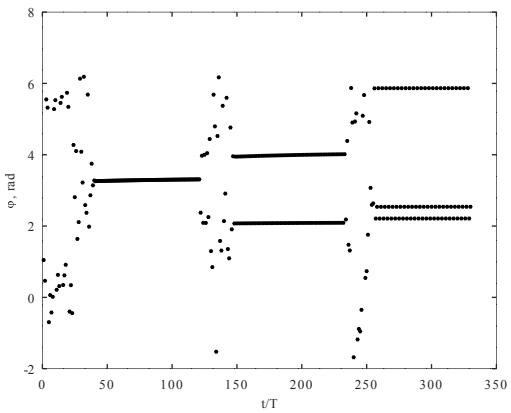

Figure 7: Control section for the UPOs Period-1, Period-2 and Period-3.

8. CONCLUDING REMARKS

This paper investigates the stabilization of unstable period orbits (UPOs) embedded in a chaotic attractor. The problem is addressed as the output tracking control of a plant with respect to some target reference trajectory. An ADRC-based controller is applied to deal with the nonlinear behavior of the system and to compensate for possible parametric uncertainties that may be present. The stability and convergence properties of the closed-loop system are also discussed. To illustrate the performance of the controller, simulation tests are performed on a chaotic pendulum. Results confirm that less controller is able to perform the stabilization. Besides, the required effort to stabilize the natural UPOs is considerable small when compared to any general unnatural orbits.

REFERENCES

Auerbach, D., Cvitanović, P., Eckmann, J.P., Gunaratne, G. and Procaccia, I., 1987. "Exploring chaotic motion through periodic orbits". *Physical Review Letters*, Vol. 58, No. 23, p. 2387.

Bessa, W.M., de Paula, A.S. and Savi, M.A., 2009. "Chaos control using an adaptive fuzzy sliding mode controller with application to a nonlinear pendulum". *Chaos, Solitons & Fractals*, Vol. 42, No. 2, pp. 784–791.

Bessa, W.M., de Paula, A.S. and Savi, M.A., 2012. "Sliding mode control with adaptive fuzzy dead-zone compensation for uncertain chaotic systems". *Nonlinear Dynamics*, Vol. 70, pp. 1989–2001.

de Paula, A.S. and Savi, M.A., 2009. "Controlling chaos in a nonlinear pendulum using an extended time-delayed feedback control method". *Chaos, Solitons & Fractals*, Vol. 42, No. 5, pp. 2981–2988.

de Paula, A.S. and Savi, M.A., 2011. "Comparative analysis of chaos control methods: A mechanical system case study". *International Journal of Non-Linear Mechanics*, Vol. 46, No. 8, pp. 1076–1089.

de Paula, A.S., Savi, M.A. and Pereira-Pinto, F.H.I., 2006. "Chaos and transient chaos in an experimental nonlinear pendulum". *Journal of sound and vibration*, Vol. 294, No. 3, pp. 585–595.

Gouvêa, J.A., Fernandes, L.M., Pinto, M.F. and Zachi, A.R.L., 2023. "Variant ADRC design paradigm for controlling uncertain dynamical systems". *European Journal of Control*, Vol. 72, p. 100822.

Hübinger, B., Doerner, R., Martienssen, W., Herdering, M., Pitka, R. and Dressler, U., 1994. "Controlling chaos experimentally in systems exhibiting large effective lyapunov exponents". *Physical Review E*, Vol. 50, No. 2, p. 932.

Jingqing, H., 1998. "Auto-disturbances-rejection controller and its applications". *Trans. Control Decis, China*, Vol. 13, No. 1, pp. 19–23.

Kapitaniak, T., 1992. "Controlling chaotic oscillators without feedback". *Chaos, Solitons & Fractals*, Vol. 2, No. 5, pp. 519–530.

Leine, R.I., 2000. *Bifurcations in discontinuous mechanical systems of Filippov-type*. Ph.D. thesis, Teknische Universiteit Eindhoven, The Nethelands.

Lu, W., Li, Q., Lu, K., Lu, Y., Guo, L., Yan, W. and Xu, F., 2021. "Load adaptive PMSM drive system based on an improved ADRC for manipulator joint". *IEEE Access*, Vol. 9, pp. 33369–33384.

Luo, S., Ma, H., Li, F. and Ouakad, H.M., 2022. "Dynamical analysis and chaos control of mems resonators by using the analog circuit". *Nonlinear Dynamics*, Vol. 108, No. 1, pp. 97–112.

Madoński, R., Gao, Z. and Łakomy, K., 2015. "Towards a turnkey solution of industrial control under the active disturbance rejection paradigm". In *54th Conf. of the Soc. of Instrum. and Cont. Eng. of Japan (SICE)*. IEEE, pp. 616–621.

Ogata, K., 2010. *Modern control engineering fifth edition*.

Ott, E., Grebogi, C. and Yorke, J.A., 1990. "Controlling chaos". *Physical review letters*, Vol. 64, No. 11, p. 1196.

Pereira-Pinto, F.H.I., Ferreira, A.M. and Savi, M.A., 2004. "Chaos control in a nonlinear pendulum using a semi-continuous method". *Chaos, Solitons & Fractals*, Vol. 22, No. 3, pp. 653–668.

Pyragas, K., 1992. "Continuous control of chaos by self-controlling feedback". *Physics letters A*, Vol. 170, No. 6, pp. 421–428.

Socolar, J.E., Sukow, D.W. and Gauthier, D.J., 1994. "Stabilizing unstable periodic orbits in fast dynamical systems". *Physical Review E*, Vol. 50, No. 4, p. 3245.

Wu, X., Jiang, D., Yun, J., Liu, X., Sun, Y., Tao, B., Tong, X., Xu, M., Kong, J., Liu, Y. *et al.*, 2022. "Attitude stabilization control of autonomous underwater vehicle based on decoupling algorithm and PSO-ADRC". *Frontiers in Bioengineering and Biotechnology*, Vol. 10, p. 843020.

Zachi, A.R.L., Correia, C.A.M., Azevedo Filho, J.L. and Gouvêa, J.A., 2019. "Robust disturbance rejection controller for systems with uncertain parameters". *IET Control Theory & Applications*, Vol. 13, No. 13, pp. 1995–2007.

Zeng, H.B., Teo, K.L., He, Y. and Wang, W., 2019. "Sampled-data stabilization of chaotic systems based on a TS fuzzy model". *Information Sciences*, Vol. 483, pp. 262–272.

Zhu, Z.Y., Zhao, Z.S., Zhang, J., Wang, R.K. and Li, Z., 2020. "Adaptive fuzzy control design for synchronization of chaotic time-delay system". *Information Sciences*, Vol. 535, pp. 225–241.